Chemical Engineering Journal 428 (2022) 131164

Contents lists available at ScienceDirect

Chemical Engineering Journal

journal homepage: www.elsevier.com/locate/cej

Phase change material microcapsules with melamine resin shell via cellulose nanocrystal stabilized Pickering emulsion in-situ polymerization

Zhe Zhang [a,b], Zhen Zhang [a,b,*], Tian Chang [a,b], Juan Wang [c], Xin Wang [a,d,*], Guofu Zhou [a,b,d,*]

[a] Guangdong Provincial Key Laboratory of Optical Information Materials and Technology & Institute of Electronic Paper Displays, South China Academy of Advanced Optoelectronics, South China Normal University, Guangzhou 510006, China
[b] SCNU-TUE Joint Lab of Device Integrated Responsive Materials (DIRM), National Center for International Research on Green Optoelectronics, South China Normal University, Guangzhou 510006, China
[c] ScienceK Ltd, Huzhou 313000, China
[d] National Center for International Research on Green Optoelectronics, South China Academy of Advanced Optoelectronics, South China Normal University, Guangzhou 510006, China

ARTICLE INFO

Keywords:
Cellulose nanocrystal
Pickering emulsion
Phase change material
Microcapsule

ABSTRACT

Thermal energy storage technology based on phase change materials (PCMs) is promising for temperature regulation and thermal energy storage. However, the applications of organic PCMs are hindered from their leakage issue. Encapsulating PCMs in microcapsules with polymer shell could effectively prevent the leakage of PCMs and enhance heat conduction. Herein, PCM microcapsules with melamine–formaldehyde resin (MF) as shell were prepared via cellulose nanocrystal (CNC) stabilized Pickering emulsion in-situ polymerization. CNCs were chosen as emulsifiers of Pickering emulsion and reinforcing nanofillers of MF shell due to their outstanding emulsifying ability, mechanical strength, and sustainability. Paraffin wax (PW) and n-octadecane (C_{18}) were employed as PCMs, respectively. The prepared PCM microcapsules are in diameter of 4 μm with a tunable thickness of MF shell. The phase change enthalpy of PW and C_{18} microcapsules are as high as 164.8 and 185.1 J/g, corresponding to PCM core material content of 87.0 and 84.3%, respectively. PCM microcapsules are stable below 200 ℃ and display a retention rate of the phase change enthalpy reach up to 99.7% after 200 cycles of heating–cooling. Moreover, the PCM microcapsules are self-extinguishing due to the flame-retardant properties of MF shell. The promising applications of PCM microcapsules in the field of temperature regulation were also demonstrated.

1. Introduction

The energy demand is dramatically increasing in recent decades due to the global population explosion and expanding economic scale. It is a constant pursuit to improve the energy utilization efficiency and seek for green energy [1–3]. During the process of energy conversion, a certain amount of energy will be inevitably lost and converted to thermal energy. A lot of heat is produced as a byproduct and wasted in many factories [4,5]. About 90% of the global energy budget involves thermal-based conversion, transport, and storage [6]. Moreover, solar energy is an extensive and green thermal energy resource. Thermal energy storage is an efficient way to fully exploit waste heat and solar-thermal energy [7]. Phase change materials (PCMs) refer to materials that can absorb or release a large amount of heat during the phase change process at a constant temperature. The heat absorbed or released during phase change is called latent heat [8,9]. The latent heat energy storage (LHES) is one of the most promising thermal energy storage approaches because of its high capacity and thermostatic energy storage process [4,10]. PCMs have been widely employed in the LHES technology to reduce the gap between energy supply and demand with respect time and space or maintain a suitable ambient temperature range during the temperate variation, such as energy-saving buildings, outdoor uninterrupted power supply (UPS), batteries, and smart textile [11–15].

The PCMs are normally classified as organic, inorganic, and eutectic PCMs with abroad phase change temperature range from -100 to 900 ℃ [16]. Among them, organic PCMs are significantly attractive for LHES

* Corresponding authors at: Guangdong Provincial Key Laboratory of Optical Information Materials and Technology & Institute of Electronic Paper Displays, South China Academy of Advanced Optoelectronics, South China Normal University, Guangzhou 510006, China.
E-mail addresses: jtzhangzhe@163.com (Z. Zhang), zhangzhen@m.scnu.edu.cn (Z. Zhang), 649199980@qq.com (T. Chang), sciencek@qq.com (J. Wang), wangxin@scnu.edu.cn (X. Wang), guofu.zhou@m.scnu.edu.cn (G. Zhou).

https://doi.org/10.1016/j.cej.2021.131164
Received 12 March 2021; Received in revised form 3 June 2021; Accepted 1 July 2021
Available online 8 July 2021

due to their relatively stable chemical properties, minimal supercooling, wide phase change temperature, and high enthalpy [17,18]. Alkanes are the most common used organic PCMs, and their phase change temperature is mainly related to the carbon numbers of alkane chains [19]. However, the intrinsic issues of organic PCMs need to be addressed for LHES applications, such as low thermal conductivity, volume expansion during the phase transition, flammability, and leakage. Microencapsulating PCMs in a shell can effectively prevent leakage during phase change and improve thermal conductivity by increasing the specific surface area between PCMs and matrices [16,20–22]. Compared with inorganic shell materials, PCM microcapsules with polymer shell have attracted many attentions due to their variety, designability, facile preparation, outstanding mechanical strength, and toughness [23–26]. Many kinds of polymers have been employed as the shell of PCM microcapsules, such as Melamine–Formaldehyde resin (MF) [23,27], polyurethane (PU) [28,29], polystyrene (PS) [24,26,30], and poly (methyl methacrylate) (PMMA) [31].

Emulsion droplets are ideal templates to fabricate PCM microcapsules, and conventional emulsions are usually emulsified by surfactants via reducing the interfacial tension between oil and water phases. However, surfactant is environment-hazardous and the abuse of surfactant have raised many environmental issues [32]. Moreover, the poor biocompatible of surfactants also hinder their applications in many fields. The removing of surfactants is costly and time-consuming, and the presence of surfactant residues sometimes can lead to severe defects of the final products [33]. Pickering emulsion is a surfactant-free emulsion stabilized by solid particles which possess partially wettability with both oil and water phase [34–36]. In conventional emulsion, surfactants adsorb and desorb at the water and oil interface on a relatively fast timescale, which is a dynamic process. However, once the solid nanoparticles are attached at the water and oil interface, a huge amount of energy is required to detach the solid nanoparticles. Therefore, compared to surfactant stabilized traditional emulsion, Pickering emulsion is more sustainable, biocompatible, and stable [34]. Pickering emulsion polymerization has been proven as an efficient approach to prepare PCM microcapsules with nanoparticle reinforced polymer shell [37,38]. The nanoparticles are employed as both emulsifiers of Pickering emulsion and reinforcing agents in the polymer shell [32,39–41]. Many solid nanoparticles have been used to prepare oil-in-water Pickering emulsion, such as SiO_2 nanoparticles [41]., graphene oxide [42,43]., chitin nanocrystals [36]., and cellulose nanocrystals (CNCs) [44].

CNCs are rod-like nanocelluloses normally extracted from wood pulp or cotton via H_2SO_4 hydrolysis. CNC has been demonstrated as an outstanding Pickering emulsifier due to its excellent emulsifying ability, renewability, biodegradability, biocompatibility, mechanical performance, good water dispersibility, and large specific surface area [45–48]. The crystals of cellulose possess both hydrophilic faces ((0 1 0)β/(1 1 0)α, (1–10)β/(1 0 0)α) and hydrophobic edge plane ((2 0 0)β/(2 2 0)α), rendering CNCs with a surfactant-like amphiphilic characteristic and excellent Pickering emulsifying ability [47,49,50]. Compared with the 0D spherical particles, the 1D rod-liked CNCs with high aspect ratio are prone to connect together and form bridge structures, leading to a dense 2D interfacial network at the interfaces. CNC stabilized Pickering emulsions have been employed as templates to fabricated PCM microcapsules. In our previous study, PCM microcapsules with CNC/PS hybrid shell were prepared via Pickering emulsion polymerization and displayed a high PCM encapsulation ratio of 83.5% [24]. However, the polymerization of styrene requires an oxygen-free environment. Therefore, air should be removed and avoided by tedious procedures during the whole preparation of Pickering emulsion and polymerization of styrene. It is a challenge to prepare the Pickering emulsion via homogenization and sonication with the absence of air. Wang et al. have reported a facile approach to fabricate PCM microcapsules with CNC/PMMA shell via Pickering emulsion assisted solvent evaporation. However, plenty of chloroform is consumed and the PCM encapsulation ratio is only 58.2% [51]. Moreover, both PS and PMMA are flammable. The formation of PS and PMMA shell is due to the insolubility and phase separation of PS and PMMA from the oil phase of Pickering emulsion, and CNCs are embedded on the surface of the PMMA and PS shells. The CNCs may detach from the PS and PMMA shells after years of use in the natural environment.

MF is one of the stiffest and hardest thermosetting resin with various excellent properties and performance, such as self-extinguishing ability, excellent boil resistance, moisture resistance, scratch resistance, and facile preparation via in-situ polymerization, [52–56]. Moreover, MF shells are formed from the water phase via in-situ polymerization and the Pickering emusifiers are incorpoareted inside the MF shells. Therefore, MF is a promising candidate as the shell of PCM microcapsules. In this study, PCM microcapsules with a diameter in several micrometer ranges were prepared via in-situ polymerization of melamine and formaldehyde with CNC stabilized Pickering emulsions as templates, leading to PCM microcapsules with CNC reinforced MF resin as the shell (Fig. 1). Paraffin wax (PW) and n-octadecane (C_{18}) with phase change temperature at about 60 and 25 ℃ were employed as the PCMs, respectively. The chemical components, morphology, thermal stability, and phase change processes of PCM microcapsules were studied by Fourier transform infrared spectra (FTIR), Polarized optical microscope (POM), Scanning electron microscope (SEM), Differential scanning calorimeter (DSC), and Thermogravimetric analysis (TGA). The self-extinguishing properties, thermal storage and regulating ability of PCM microcapsules were also demonstrated.

2. Experimental section

2.1. Materials

PW, C_{18}, melamine, and formaldehyde (37 wt% in water) were purchased from Adamas. CNCs were provided by ScienceK Ltd. (www.sciencek.com). Hydrochloric acid and sodium hydroxide were obtained from Guangzhou Reagent. Sodium chloride was obtained from Tianjin Zhiyuan Chemical Reagent. Poly (vinyl alcohol) (AR, 1788) was obtained from General-reagent.

2.2. Preparation of CNC stabilized Pickering emulsions

The CNC stabilized PW or C_{18} Pickering emulsions were achieved through ultrasonication. In detail, the CNC aqueous suspension (0.5 wt %) was prepared by dispersing CNC powders in distilled water via homogenization and ultrasonication. NaCl (0.5 wt%) was added to the CNC aqueous suspension to shield the ionic strength of CNCs. PW or C_{18} (36 g) was added to CNC aqueous suspension (84 g) and then the mixture was heated to melt PCMs. The CNC stabilized PCM emulsions were prepared via ultrasonication for 15 min under the power of 650 W by an ultrasonic cell disruptor (Ningbo Xinzhi Co., Ltd, JY92-IIN).

2.3. Preparation of the PCM microcapsules with CNC and MF hybrid shell

The PCM microcapsules with CNC and MF hybrid shells were prepared via Pickering emulsion in-situ polymerization of MF precursor. In detail, melamine (2.52 g) and formaldehyde (4.86 g) were added to 15 ml deionized water in a flask, and then the pH of the mixture was adjusted to 8 ~ 9 by adding NaOH (1 mol/L). After the reaction was conducted at 70 ℃ for 30 min, a clear MF precursor was obtained. The CNC stabilized Pickering emulsions (120 g) prepared in the last step were diluted with deionized water (100 g), and the pH was adjusted to 3 ~ 4 by adding HCl (1 mol/L). Then the MF precursor was added dropwise into the diluted PCM Pickering emulsions. The Pickering emulsion in-situ polymerization of MF precursor was conducted at 70 ℃ for 3 h, leading to PCM microcapsule slurries. The PCM microcapsule powders were obtained via suction filtration of PCM microcapsule slurries, washing with water, and dried at 40 ℃ overnight.

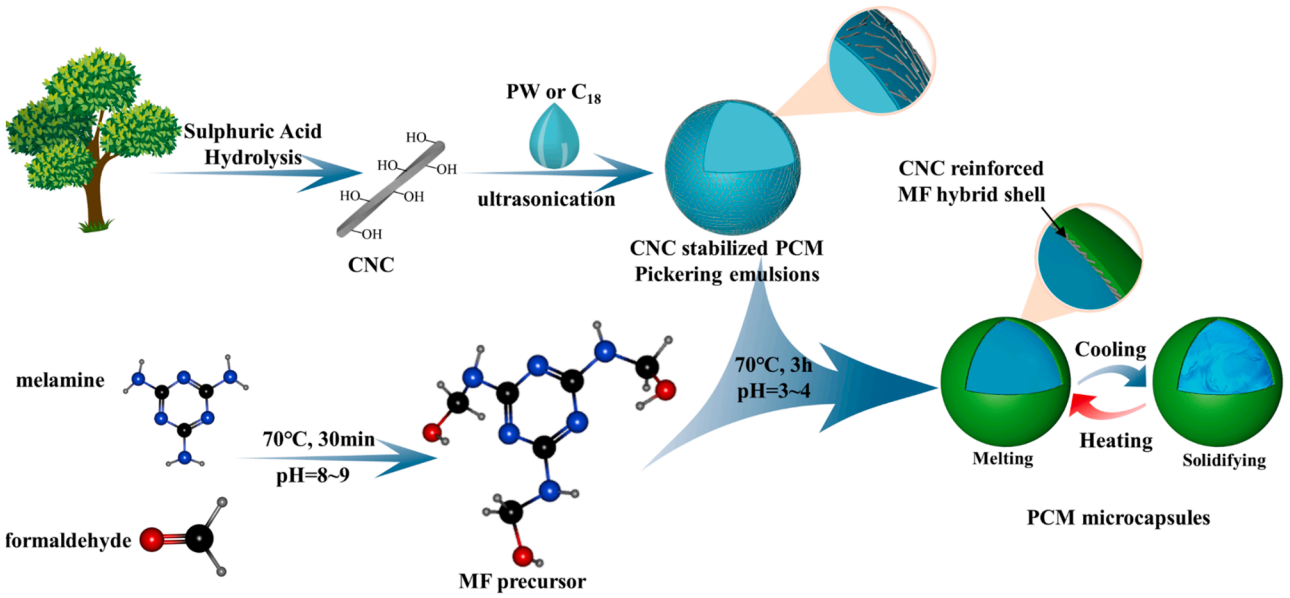

Fig. 1. Schematic illustration of the preparation of PCM microcapsules with CNC reinforeced MF hybrid shell.

2.4. Preparation of the C_{18}/PVA film

The C_{18}/PVA film was prepared via solution casting. PVA solution (20 wt%) was obtained by dissolve PVA (2 g) in deionized water (8 ml) under stirring at 70 ℃ for 3 h. Then C_{18} microcapsule slurries (net weight of C_{18} microcapsules is 2 g) were added into the molten PVA solution, and the mixture was poured into a Petri dish. After drying at 45 ℃ for 12 h, C_{18}/PVA film was obtained. The weight ratio of C_{18} microcapsules to PVA was fixed at 1:1. A neat PVA film of 4 g was also prepared with a similar procedure.

2.5. Characterization

The morphologies of the PCM Pickering emulsions and microcapsules were examined using a polarized optical microscope (POM, DM2700P) and a field-emission scanning electron microscope (SEM, ZEISS Gemini 500). In order to characterize the shell thickness and internal morphology of the PCM microcapsules, PCM microcapsules slurries were mixed with varnish and dried in a Petri dish at room temperature. After frozen in liquid nitrogen, the PCM microcapsules and varnish film were brittle and broken easily. The cross-section of the fracture was then observed by SEM.

The thermal stability of PCMs was evaluated by TGA (Mettler Toledo, TGA2). PCM samples were heated from 25 ℃ to 800 ℃ at a heating rate of 10 ℃/min under N_2 atmosphere.

Fourier transform infrared spectra (FTIR) were conducted with Nicolet 6700.

The phase change processes of PCMs were studied by differential scanning calorimetry (DSC, Mettler Toledo DSC1). The PCM samples were heated or cooled at a rate of 5 ℃/min in the range of 10 ~ 80 ℃ (for PW samples) and −10 ~ 60 ℃ (for C_{18} samples) under the N_2 atmosphere. In order to erase the thermal history, the first heating scan was not recorded. Moreover, 200 heating and cooling cycles of the PCM samples were performed to evaluate the durability of PCM microcapsules.

The phase change temperature was determined by the intersection of the baseline and tangent with the maximum slope. The latent heat of PCMs is calculated by numerical integration of the area under the peaks. The PCM core material content (E_c) and encapsulation efficiency (E_p) are estimated by the following eqs. (1) and (4), respectively.

$$E_c = \frac{\Delta H_m + \Delta H_c}{\Delta H_{m0} + \Delta H_{c0}} \times 100\% \quad (1)$$

$$m_{MF} = n_{melamine} \times \left(M_{MFprecursor} - M_{H_2O} \times 3\right) \quad (2)$$

$$\varphi_{PCMs} = \frac{m_{PCMs}}{m_{PCMs} + m_{MF} + m_{CNCs} + m_{NaCl}} \times 100\% \quad (3)$$

$$E_p = \frac{E_c}{\varphi_{PCMs}} \quad (4)$$

where the ΔH_{m0} and ΔH_{c0} are the melting and solidifying enthalpies of bulk PCMs, ΔH_m and ΔH_c represent the enthalpies of the PCM microcapsules during melting and solidifying. Assuming the yield of in-situ polymerization is 100% [57]., the theoretical yield was calculated by equation (2) and φ_{PCMs} is the theoretical mass fraction of PCMs to PCM microcapsules, respectively.

3. Results and discussion

3.1. Preparation of CNC stabilized PCM Pickering emulsions

CNCs show excellent Pickering emulsifying ability due to their partial wettability with both oil and water phases [45,47]. The CNCs used in the study are extracted from wood pulp by sulfuric acid hydrolysis and are [37] negatively charged due to the presence of sulfuric ester groups. The electrostatic repulsion among CNCs hinder them to immobilize at the interface between water and oil. Therefore, NaCl is added to the CNC dispersion to shield the ionic strength of CNCs and faciliate the formation of Pickering emulison [37]. The concentrations of CNCs and NaCl of aqueous dispersion were fixed at 0.5 wt%, and PW and C_{18} Pickering emulsions were prepared via sonication by ultrasonic cell disruptor. Fig. 2a and d show the optical images of PW and C_{18} Pickering emulsions, respectively. After 6 months of storage, no obvious phase separation was found, indicating a good stability of CNC stabilized PCM Pickering emulsions. The morphology of the PW and C_{18} Pickering emulsions were observed by POM at room temperature, as shown in Fig. 2b and e, respectively. The size of over 800 emulsion droplets was counted, and the size distribution was shown in Fig. 2c and f. The size of both PW and C_{18} Pickering emulsions are quite uniform and mainly ranging from 2 to 6 μm, and can be easily tuned by varying the concentration of CNCs [37].

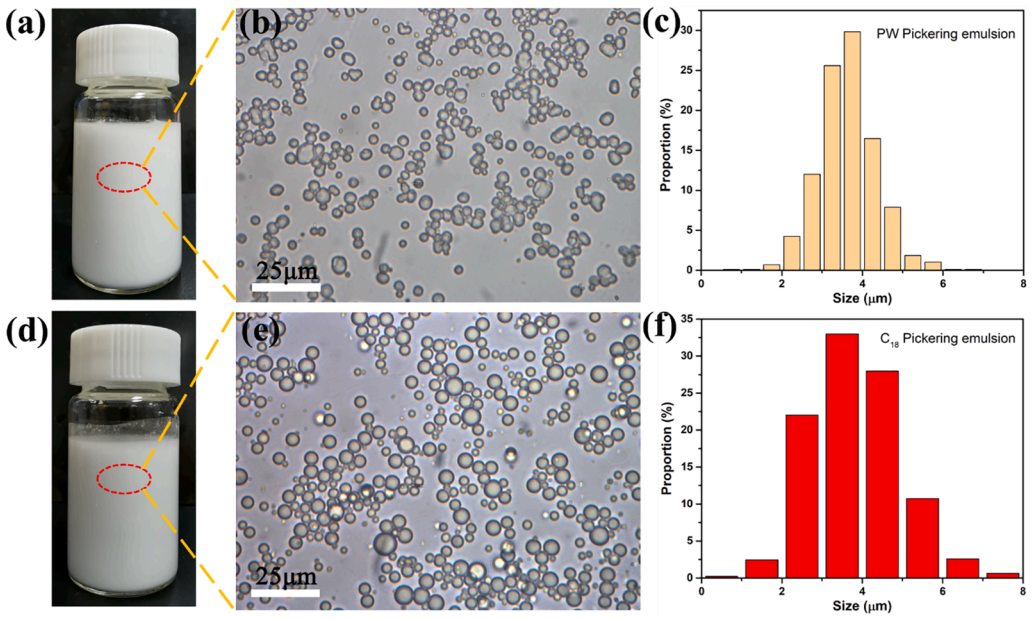

Fig. 2. (a) PW and (d) C_{18} Pickering emulsions after 6 months; POM images and particle size distribution of PW (b, c) and C_{18} Pickering emulsions (e, f).

Interestingly, it is found that the emulsion droplets of PW Pickering emulsion are irregular spheres, while the sphere shape of C_{18} Pickering emulsion droplets is almost perfect at room temperature. We assumed the regularity of the PCM Pickering emulsion droplets may be related to the relationship between the phase change temperature of PCMs and room temperature. To verify this assumption, the optical microscopes of PCM Pickering emulsions were observed under different temperatures. As shown in Fig. 3a, the PW Pickering emulsion droplets are irregular sphere at 25 and 35 ℃, then become almost perfect sphere at 55 and 65 ℃. When the temperature is cooled to 25 and 35 ℃, the PW Pickering emulsion droplets turn to irregular sphere again. The shape change of PW Pickering emulsion droplets with temperature is reversible many times without broken, suggesting a stable Pickering emulsion. The PW begins to melt at about 45 ~ 50 ℃ and is mainly in a liquid state at 55 and 65 ℃. As the volume of PW in the liquid is larger than that in the solid state, the PW Pickering emulsion droplets display a regular sphere at a temperature higher than the melting point and an irregular sphere at temperature lower than the freezing point. The C_{18} Pickering emulsion shows a similar sphere shape change with temperature as PW Pickering emulsion. As shown in Fig. 3b, the C_{18} Pickering emulsion droplets are regular sphere at a temperature above 30 ℃ and irregular sphere at a temperature below 25 ℃. Therefore, PCM microcapsules with a regular spherical and dense structure should be obtained by preparing shells above phase transition temperature.

3.2. Preparation of PCM microcapsules with MF shell

Although the CNC stabilized PCM Pickering emulsions show excellent stability during storage and heating–cooling cycles, the emulsion is still in a metastable state [24,47]. Demulsification will occur eventually after a long enough period, evaporation of all the water, or in an extreme environment. The CNC stabilized PW Pickering emulsion was dried at room temperature to obtain PW droplets and then heated at 70 ℃ with different time (0 min, 1 min, and 1 h) for observation by SEM (Fig. 4). The pristine PW droplets at dry state possessed a spherical droplet shape. After being heated at 70 ℃ for 1 min, the PW droplets began to merge above the melting point of PW; after being heated at 70 ℃ for 1 h, the PW was totally merged together and PW droplets were disappeared. Therefore, the CNC stabilized PW Pickering emulsion at dry state is not stable, and it is necessary to form a more stable shell outside the PCM Pickering emulsion droplets.

The PCM microcapsules with MF shell were fabricated via Pickering emulsion in-situ polymerization of MF precursor with CNC stabilized PCM Pickering emulsions as templates. The obtained PW (Fig. 5a) and C_{18} (Fig. 5e) microcapsules with MF shell were observed by POM, and the size distributions of PW and C_{18} microcapsules are shown in Fig. 5d

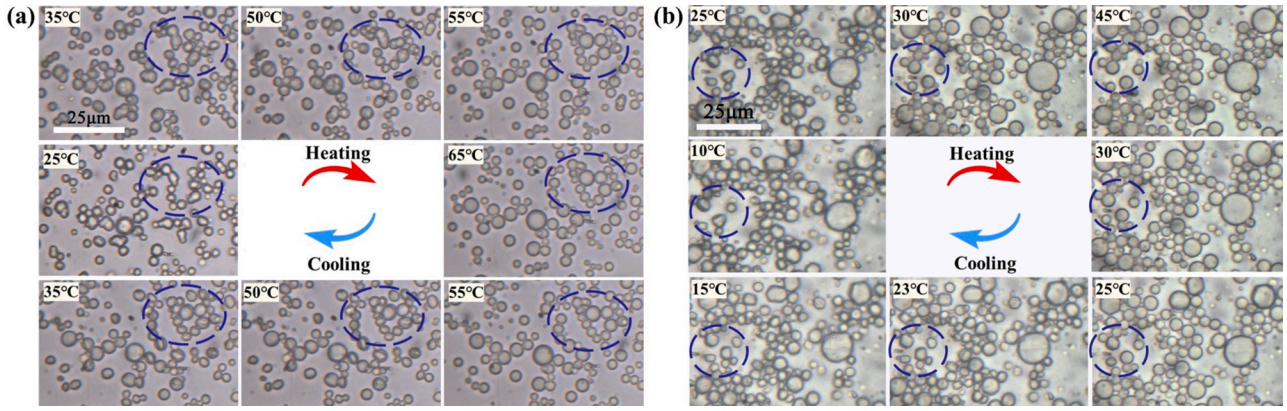

Fig. 3. The POM images of PW (a) and C_{18} (b) Pickering emulsions were observed at different temperatures.

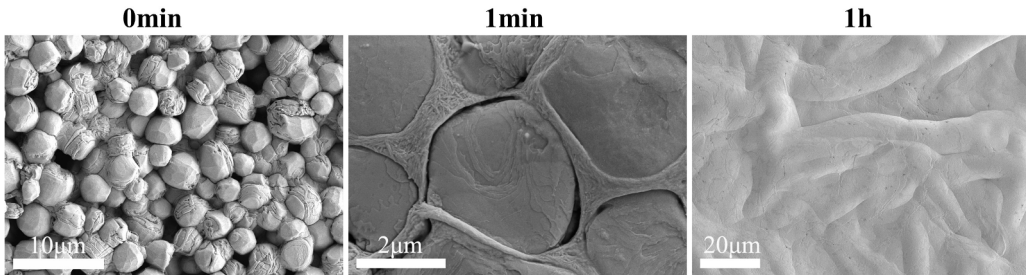

Fig. 4. The SEM image of PW Pickering emulsion with different time periods at 70 ℃.

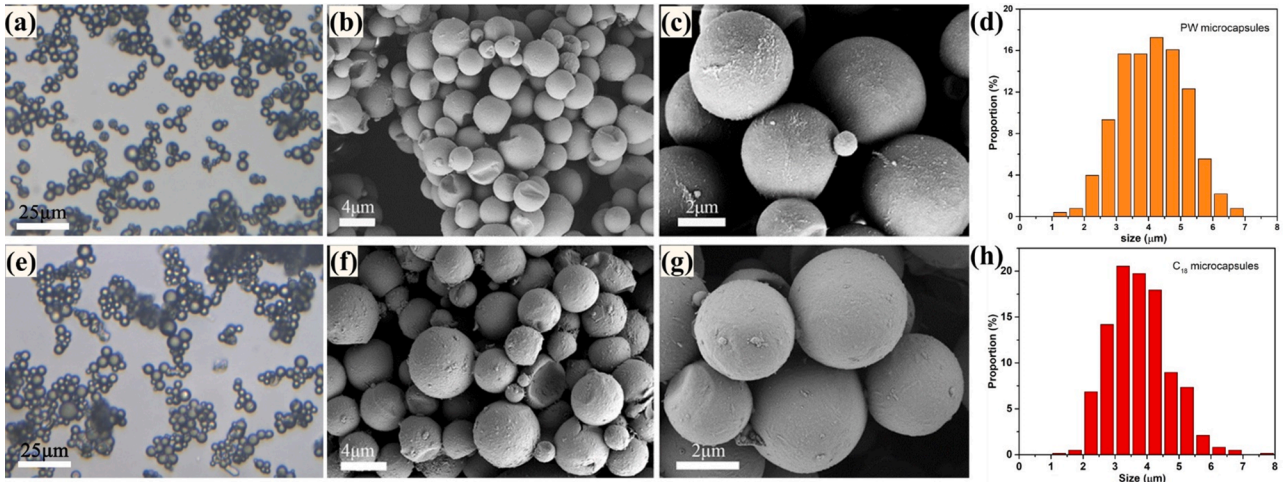

Fig. 5. POM images of PW (a) and C_{18} (e) microcapsules; SEM images of PW (b, c) and C_{18} (f, g) microcapsules at different magnifications; the particle size distribution of PW (d) and C_{18} (h) microcapsules.

and h, respectively. The PCM microcapsules remain a similar size as Pickering emulsion droplets after covering the MF shell. However, slight flocculation was found among adjacent PCM microcapsules, and the PCM microcapsules were prone to cream in several days. The slight flocculation of PCM microcapsules should be related to the disappearance of electrostatic repulsion among CNC stabilized Pickering emulsions after the formation of MF shell. SEM was also used to characterize the morphology of the PW (Fig. 5b and c) and C_{18} (Fig. 5f and g) microcapsules. The PCM microcapsules display a spherical shape with a dense MF shell, and the small dents observed on the surface of PCM microcapsules may be caused by the volume change of PCMs during solidification. In our previous study, CNCs were obviously found on the surface of PCM microcapsules with PS shell prepared via the Pickering emulsion polymerization of styrene in the oil phase [24]. However, no CNCs were observed on the surface of PCM microcapsules with MF shell, as CNCs were incorporated inside the MF shell via the Pickering emulsion in-situ polymerization approach. The hydrophilic CNCs around the PCM droplets could prevent the leakage of PCM during phase change, and the CNC incorporated MF resin is expected with high mechanical properties than neat MF resin.

The FTIR spectra of the CNCs, PW, C_{18}, MF, and PCM microcapsules are shown in Fig. 6. CNCs show typical vibrations of cellulose at 3500–3200, 2901, 1300–1400, and 1000–1150 cm^{-1}, which are associated with the O–H stretching vibration, asymmetric C–H stretching vibration, C-O–H bending, and -O- bending, respectively. MF displays vibration at 3306, 1300–1500, 996, and 810 cm^{-1}, which are attributed to the N–H stretching vibrations of a secondary amine, the methylene C–H bending vibration, the C–H out of plane deformations, and bending vibration of triazine ring, respectively. PW and C_{18} show typical FTIR spectra of alkanes, such as the symmetrical stretching vibration of –CH, $–CH_3$, and $–CH_2$ at 2955, 2915, and 2847 cm^{-1}, deformation vibration of

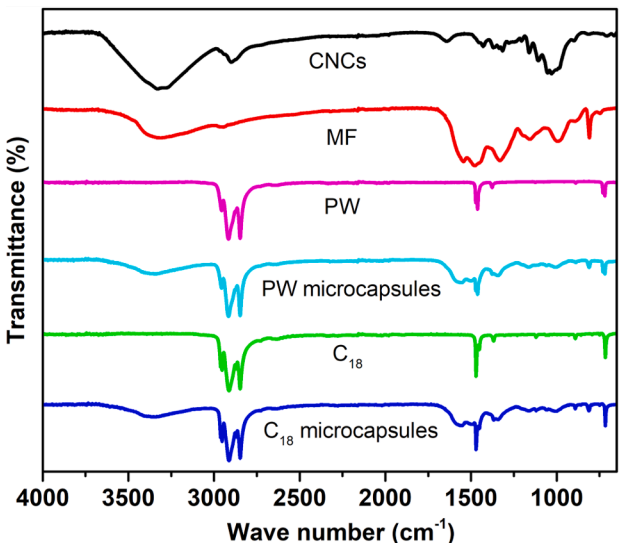

Fig. 6. FTIR spectra of CNCs, MF, PW, C_{18}, and PCM microcapsules.

$–CH_2$ and $–CH_3$ at 1461 cm^{-1}, and rocking vibration of $–CH_2$ at 719 cm^{-1}. The PCM microcapsules display the characteristic vibration of PCMs, CNCs and MF, and no new vibration appears, suggesting that there is no chemical reaction between the MF shell and the PCM core materials.

In order to further study the structure of PCM microcapsules, the cross-section of PW microcapsules prepared via brittle fracture method was characterized by SEM, as shown in Fig. 7. The PW microcapsules

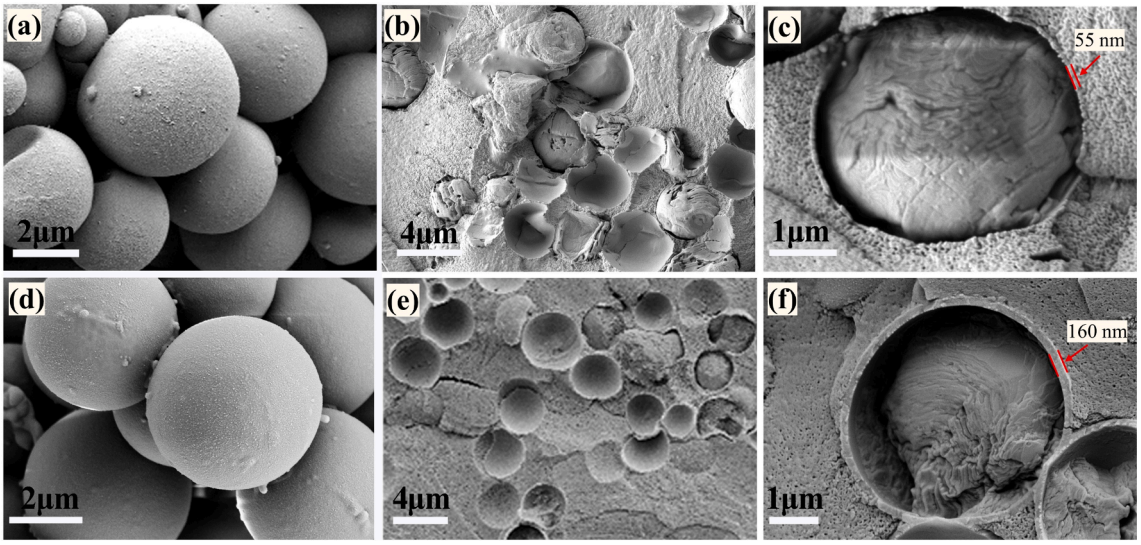

Fig. 7. The SEM images of PW (a) and PW3MF (d) microcapsules; The cross-section images of PW (b, c) and PW3MF (e, f) microcapsules at different magnifications.

show core–shell structure, and an obvious gap between PW core and MF shell is observed, which reserves space for the volume change during the phase change of PW. According to the SEM images, the thickness of MF shell of PW microcapsules is about 55 nm (Fig. 7c). And the thickness of MF shell could be well tuned by changing the amount of MF precursor. When three times amount of MF precursor was employed for Pickering emulsion in-situ polymerization to prepare PW3MF microcapsules, the MF shell with a thickness of 160 nm was achieved (Fig. 7f). A thicker MF shell could provide more mechanical strength but decrease the PCM contents of PCM microcapsules. Therefore, the thickness of MF shell should be well tuned according to the specific application to keep an appropriate balance between mechanical strength and PCM contents.

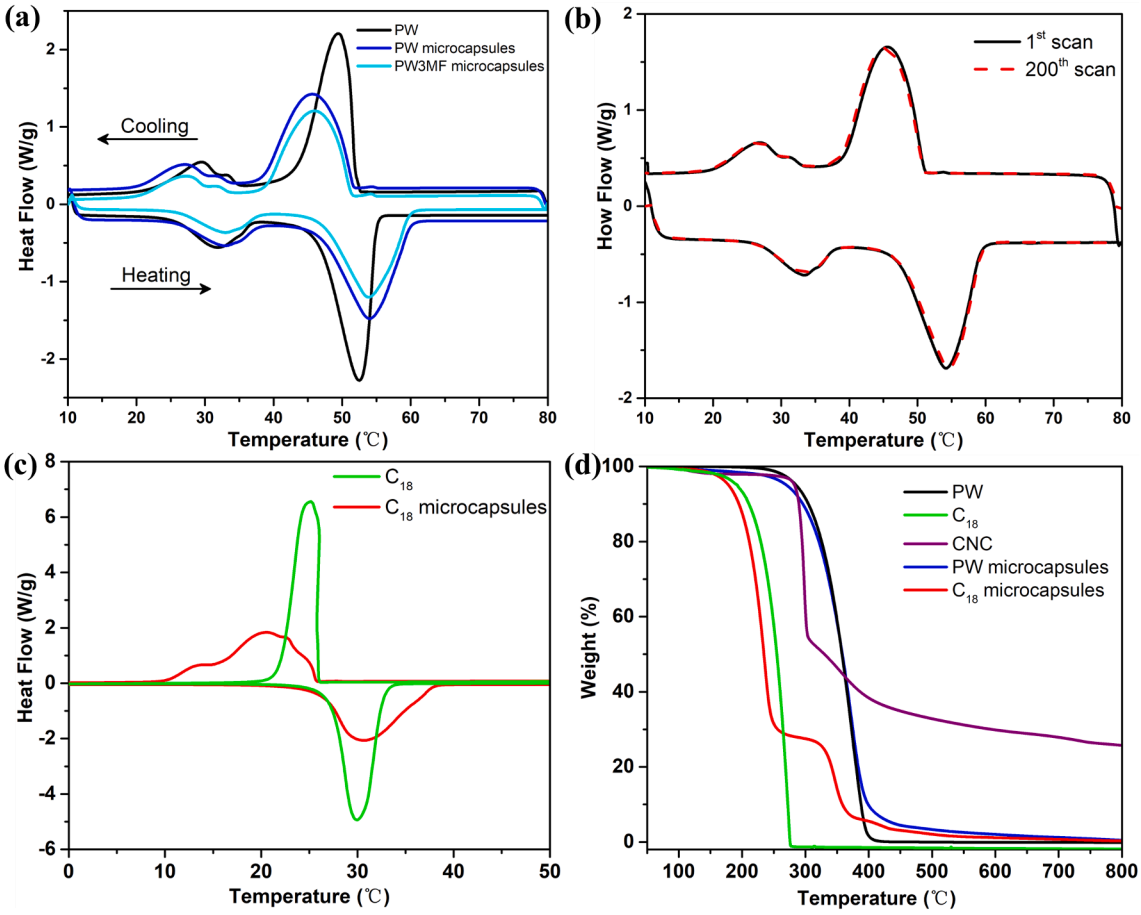

Fig. 8. (a) DSC curves of bulk PW, PW and PW3MF microcapsules. (b) DSC curves of PW microcapsules at the first (black line) and 200th (red line) heating–cooling scans. (c) DSC curves of bulk C_{18} and C_{18} microcapsules. (d) TGA curves of CNC, PW, C_{18}, and PCM microcapsules. (For interpretation of the references to colour in this figure legend, the reader is referred to the web version of this article.)

3.3. The phase change properties of PCM microcapsules

DSC analyses were performed to evaluate the phase change properties of PCM microcapsules, such as melting or solidifying temperature and latent heat storage capacity. The DSC scans of bulk PW and PW microcapsules are shown in Fig. 8a. The phase change behavior of bulk PW possessed two phase-change peaks in both the heating and cooling scans. The small peak at lower temperature ranges represents the solid–solid transition from an ordered phase to a more disordered rotator phase, while the big peak at higher temperature ranges denotes the solid–liquid melting process [58,59]. The thermal properties of PW, C_{18}, and PCM microcapsules are summarized in Table 1. The melting and solidifying temperatures of PW approximately in the range of 23.02–55.49 ℃ and 52.69–19.29 ℃, respectively. The latent heat of melting and freezing of bulk PW was measured as 186.12 and 192.78 J/g, respectively. The DSC curves of both PW and PW3MF microcapsules also display two change peaks during the phase change.

The phase change behavior of PW and PW3MF microcapsules are similar to bulk PW, as there is no chemical reaction between PW and MF shell during the preparation of PCM microcapsules. The T_{endset} of PW microcapsules was about 5 ℃ higher than that of bulk PW during the melting process, and T_{onset} of PW deceased about 1 ℃ after microencapsulation within MF shell during the solidifying process. This may be related to the size of PW microcapsules, as the number of nuclei in each capsule reduces with the decrease of capsule size, leading to a slightly increased supercooling of microcapsules [28,60,61]. The PCM core material content (E_c) and encapsulation efficiency (E_p) of PW microcapsule are calculated according to Eqs. (1) and (4), and are summarized in Table 2. The melting and freezing enthalpy of PW microcapsule is 163.02 and 166.63 J/g, respectively. Therefore, the E_c of PW microcapsule is as high as 87.0%, which is higher than the E_c (83.5%) of the PW microcapsule with PS shell prepared in our previous research. PW3MF microcapsules show a lower E_c about 76.4% due to the thicker MF shell. Both PW and PW3MF microcapsules display a quite high E_p about 96.6% and 98.8% respectively.

The DSC curves of bulk C_{18} and C_{18} microcapsules are presented in Fig. 8c. Bulk C_{18} shows only one narrow endothermic or exothermic peak in its heating or cooling DSC curves. At the beginning of solidifying process, bulk C_{18} even shows slightly increased temperature with time at around 26 ℃, as the bulk C_{18} with high purity releases a lot of heat during the solidifying in a short time. In addition, the phase transition temperature range becomes significantly wider after the formation of microcapsules, especially during the cooling process, as the MF shell delays the crystallization of C_{18}. As shown in Table 1, the latent heats of melting and solidifying of bulk C_{18} are 217.45 and 212.84 J/g, respectively. Meanwhile, the latent heat of melting and solidifying of C_{18} microcapsule were 184.64 and 185.61 J/g, respectively. The E_c of C_{18} in microcapsules is 84.3%, leading to an E_p of 93.9%.

Table 2
The φ_{PCM}, Ec, Ep of PCM microcapsules.

Sample name	MF (g)	CNC/NaCl (g)	PCM (g)	φ_{PCM}(%)	Ec (%)	Ep (%)
PW microcapsules	3.24	0.84	36	89.8	87.0	96.6
PW3MF microcapsules	9.72	0.84	36	77.3	76.4	98.8
C_{18} microcapsules	3.24	0.84	36	89.8	84.3	93.9

3.4. Thermal reliability of PCM microcapsules

Thermal stability is a crucial factor affecting the service life of PCM microcapsules and products. The thermal cycling stability of PCM microcapsules was assessed via 200 heating–cooling thermal cycles by DSC, as shown in Fig. 8b. The retention rate of phase change enthalpies for PW microcapsule can be estimated according to the following equation:

$$\text{retention rate} = \frac{\Delta H_0 - \Delta H_t}{\Delta H_0} \times 100\% \quad (5)$$

where ΔH_0 and ΔH_t are the enthalpies of PW microcapsule before and after 200 heating-cooling thermal cycles, respectively. The PW microcapsules display almost the same phase change enthalpy after 200 heating–cooling thermal cycles, and the retention rate of ΔH reach up to 99.7%. Therefore, PW microcapsules with MF shell exhibit good thermal reliability during the phase change process.

Thermal degradation behaviors of bulk PW, bulk C_{18}, and PCM microcapsules were analyzed by TGA as in Fig. 8d. All the samples were stable below 200 ℃, and both bulk PW and PW microcapsules displayed a typical single weight loss from 307 ℃ to 399 ℃ due to PW evaporation and MF degradation. Bulk C_{18} exhibited only one thermal decomposition process from 207 to 276 ℃ due to the evaporation of C_{18}. C_{18} microcapsules displayed two thermal decomposition processes in the TGA curves. The first decomposition process from 200 to 256 ℃ is due to the evaporation of C_{18}, while the second decomposition process from 333 to 443 ℃ is related to the decomposition of the MF shell.

The leakage of PW microcapsules at high temperature was also checked via filter paper. As shown in Fig. 9, the bulk PW and PW microcapsules were placed on filter papers at 100°C for 12 h. The bulk PW began to melt immediately, and the whole filter paper was totally soaked by the melted PW. However, no PW leakage was observed for PW microcapsules even after 12 h. Several drops of red dye were dropped on the filter paper in order to visualize the leaked PW. The filter paper with bulk PW cannot be stained as it becomes hydrophobic due to the infiltration of PW, while the filter paper with PW microcapsules can be completely stained, indicating no PW leakage.

3.5. Thermal storage and thermo-regulating performance of PCM microcapsules

In order to test the actual thermal energy storage capacity of PW

Table 1
Thermal properties of PW, $C_{18,}$ and PCM microcapsules.

Sample name		Melting				Solidifying			
		T_{onset}[a] (℃)	T_{peak}[b] (℃)	T_{endset}[c] (℃)	ΔHm (J/g)	T_{endset}[c] (℃)	T_{peak}[b](℃)	T_{onset}[a] (℃)	ΔHc (J/g)
PW		23.02	52.53	55.49	186.12	19.29	49.52	52.69	192.78
PW microcapsules	1st scan	24.72	54.24	60.21	163.02	19.32	45.49	51.26	166.63
	200th scan	25.34	54.63	60.58	163.01	19.39	45.24	51.07	165.52
PW3MF microcapsules		24.64	53.92	60.38	141.88	18.98	46.00	51.46	147.66
C_{18}		25.70	25.17	33.37	217.45	21.01	29.97	25.96	221.84
C_{18} microcapsules		24.15	20.51	38.50	184.64	9.57	30.69	25.70	185.61

[a] T_{onset}: Phase transition onset temperature during melting or solidifying process.
[b] T_{peak}: Melting or crystallization temperature.
[c] T_{endset}: Phase transition end temperature during melting or solidifying process.

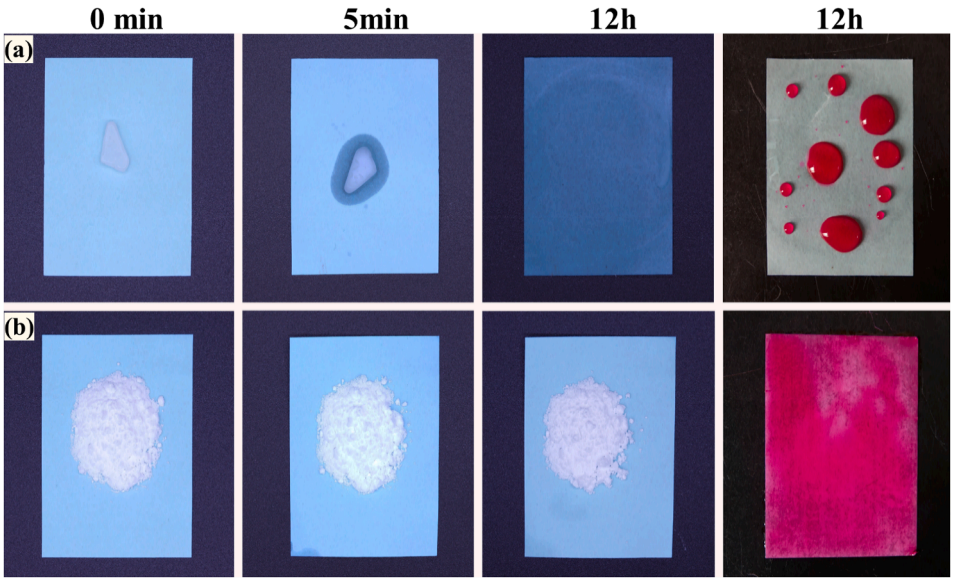

Fig. 9. The leak test analysis of bulk PW (a) and PW microcapsules (b).

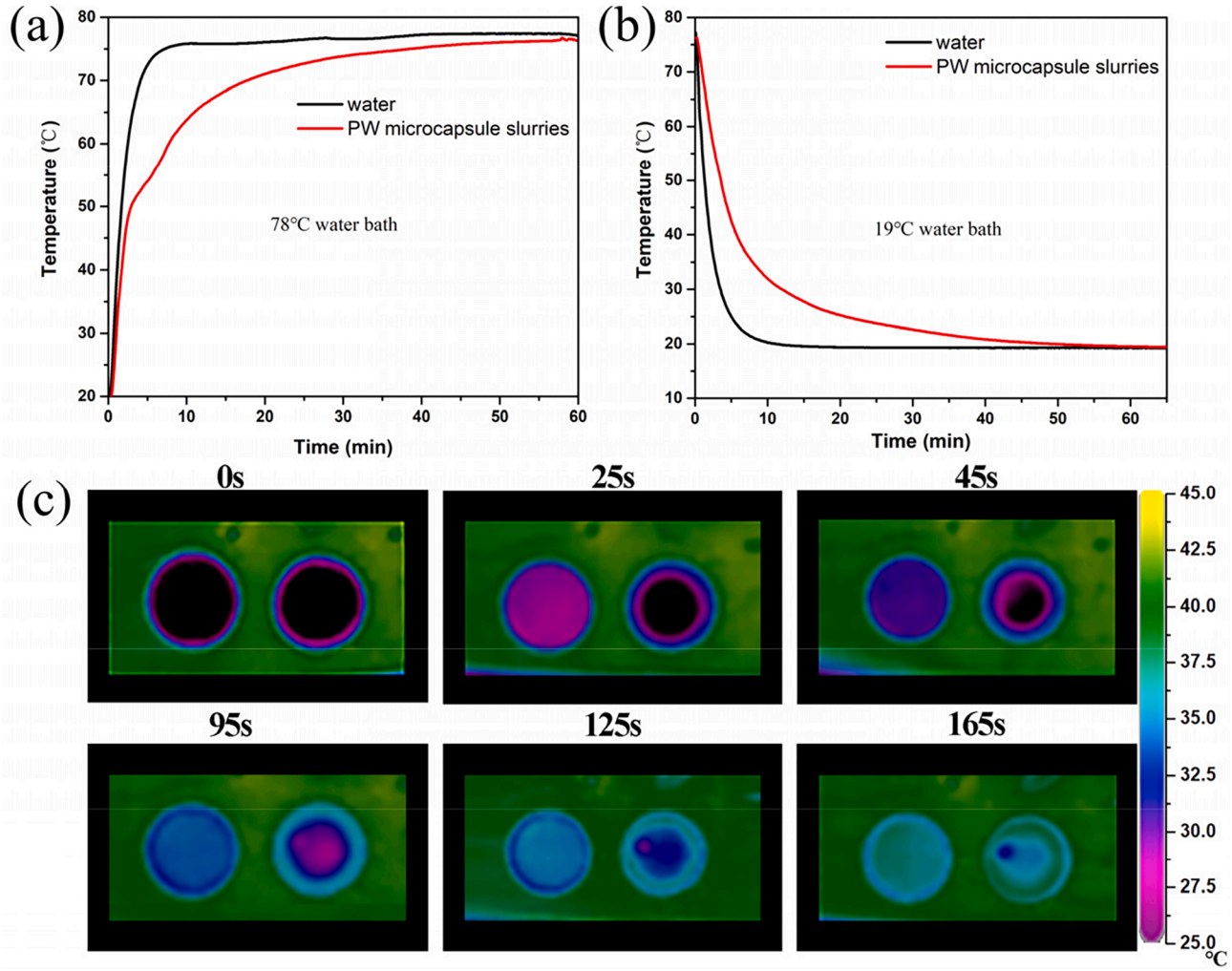

Fig. 10. Temperature regulation of water and PW microcapsule slurries when heating at 78 ℃ (a) and cooling at 19 ℃ (b); (c) infrared thermography photos showing the surface temperature increments of neat PVA film (left) and C_{18}/PVA film (right) at different heating times.

microcapsules, 50 g PW microcapsule slurries with a mass fraction of 23% were employed as temperature regulator with water as a reference. The PW microcapsule slurries and water were simultaneously placed in a 78 ℃ bath and their temperature were recorded to compare their heat storage performance, as showed in Fig. 10a. During the heating process, the temperature of the water rose rapidly from 20 to 75 ℃ in 7 min, while it took 40 min for the PW microcapsule slurries. When the PW microcapsule slurries temperature reached 50 ℃, the heating rate begins to slow down due to the phase transition of PW. When the temperature of the water bath is 19 ℃, the temperature of slurries and water reference were also recorded, as shown in Fig. 10b. The water reference dropped to 21 ℃ from 77 ℃ within 8 min, while it took 39 min for PW microcapsule slurries at the same conditions. Warm boiled water is preferred for drinking in many countries. When PW microcapsule is applied as the insulation layer of a thermos cup, 100 g PW microcapsule powders can absorb about 16 kJ of heat energy when it rises from 25 to 60 ℃, which can decrease the temperature of 100 g of water from 100 to 60 ℃. When the temperature of water drops below 60 ℃, the PW microcapsules start to release heat energy, which could extend the storage time of water in a warm and drinkable temperature range.

The thermo-regulating performance of C_{18} microcapsule was also evaluated. C_{18}/PVA film prepared by solution casting was cooled to 0 ℃ in the fridge, and then was placed onto a hotplate at a temperature of 45 ℃. The temperature of C_{18}/PVA film was recorded with time by an infrared thermal imager, while a neat PVA film was employed as a reference, as shown in Fig. 9c. After heating for 95 s, the temperature of C_{18}/PVA and neat PVA films (at the core) are about 26 and 38 ℃, respectively. The heating rate of the C_{18}/PVA film was much slower than that of the neat PVA films, suggesting a significant temperature regulation ability of C_{18} microcapsules.

3.6. Self-extinguishing of PW microcapsules

MF resin is an intrinsic flame-retardant with good resistance and self-extinguishing. Due to the triazine rings, MF will decompose at high temperature, release a lot of N_2 and form coke layers to slow combustion [57,62]. The flame retardant performance of PW microcapsule was verified through high temperature heating and candle burning experiments. The bulk PW and PW microcapsules of the same quality were placed on the asbestos gauze and heated with an alcohol lamp. As shown in Fig. 11a and video S1 of supporting information, the bulk PW melted rapidly at high temperatures and infiltrate the asbestos gauze to start burning. However, no fire was observed when PW microcapsules were heated by an alcohol lamp. The morphology of PW microcapsule after combustion was observed by SEM, as showed in Fig. 11d. The MF shell of PW microcapsule was still retained after burning, suggesting a good fire resistance of PW microcapsule. In addition, bulk PW and PW microcapsules were filled into beakers as home-made candles for the combustion test, as shown in Fig. 11b, c and video S2 (supporting information). After ignition of cotton thread, the candle with bulk PW can keep burning, while the candle with PW microcapsule was extinguished after several minutes. During the combustion process of MF, nitrogen was released and a carbonized layer was formed on the surface, which can block the oxygen and lead to self-extinguishing.

4. Conclusion

Microencapsulating organic PCMs in polymer shell is an effective approach to prevent the leakage issue. In this study, The CNC stabilized Pickering emulsions were employed as templates to fabricate PCM microcapsules with MF resin shell through in-situ polymerization. Both PW and C_{18} with phase change temperature at about 60 and 25 ℃ were employed as PCMs. CNCs were used as both Pickering emulsifiers and reinforcing nanofillers due to their excellent emulsifying ability, renewability, biodegradability, and mechanical strength. The PCM Pickering emulsion droplets stabilized by CNCs are regular spheres at temperature higher than its phase change temperature and become shrunken spheres at temperature lower than its phase change temperature, due to the volume change of PCMs during phase change. The MF shell was formed via Pickering emulsion in-situ polymerization of precursor, leading to PCM microcapsules with CNC reinforced MF shell. The thickness of MF shell of PCM microcapsules could be well-tuned by the amount of MF precursor. The PW microcapsules possess a phase change enthalpy of 164.8 J/g, corresponding to a PCM core material content of 87.0%. Compared with water, PW microcapsule slurries show a better thermal management effect. C_{18} microcapsules display a phase change enthalpy of 185.1 J/g, corresponding to a PCM core material content of 84.3%. The PVA film incorporated with C_{18} microcapsule shows much better temperature regulation ability than neat PVA film. The PCM microcapsules are thermal stable under 200 ℃ and there is no leakage of PCM at 100 ℃ for 12 h. Even after 200 cycles of heating–cooling at the temperature of 10 to 80 ℃, the retention rate of phase change enthalpy

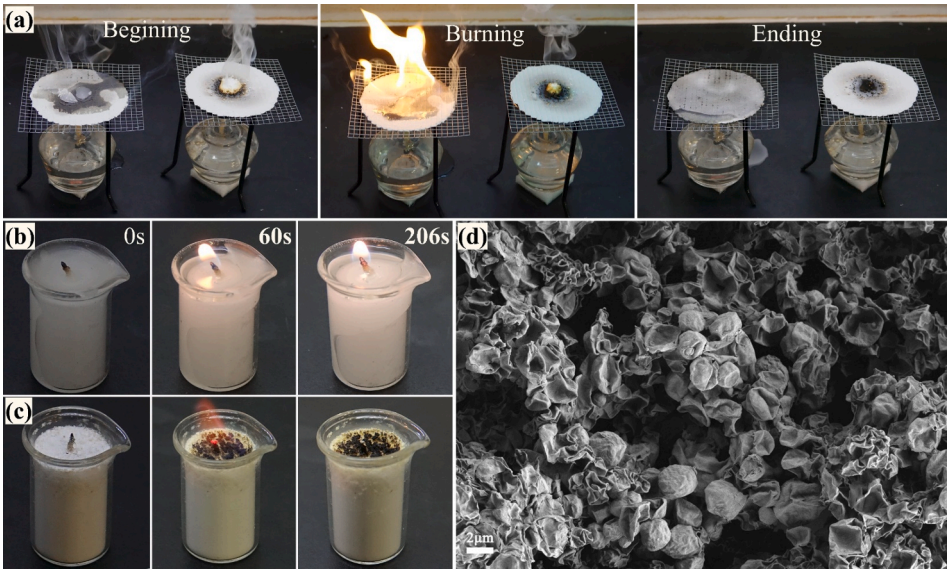

Fig. 11. (a) The high temperature heating test of bulk PW (left) and PW microcapsules (right) use an alcohol lamp; the self-extinguishment test of bulk PW (b) and PW microcapsules (c) candles; (d) SEM image of PW microcapsules after combustion by an alcohol lamp.

of PW microcapsule is as high as 99.7%. Moreover, PCM microcapsules are self-extinguishing due to the fire-retardant properties of MF shell, making them quite promising for thermal energy storage.

Declaration of Competing Interest

The authors declare that they have no known competing financial interests or personal relationships that could have appeared to influence the work reported in this paper.

Acknowledgments

The authors wish to acknowledge the funding support from Natural Science Foundation of Guangdong Province (1914050005542), Grand of 2019 Guangdong Recruitment Program of Foreign Experts (191900014), ScienceK, Science and Technology Program of Guangzhou (No. 2019050001), Guangdong Provincial Key Laboratory of Optical Information Materials and Technology (No. 2017B030301007), Guangdong University Research Findings Commercialization Center and Education Bureau of Foshan Innovation Research Program (2020JNHB09), and Yunnan expert workstation (202005AF150028).

Appendix A. Supplementary data

Supplementary data to this article can be found online at https://doi.org/10.1016/j.cej.2021.131164.

References

[1] I. Dincer, Renewable energy and sustainable development: a crucial review, Renew. Sust. Energ. Rev. 4 (2) (2000) 157–175.
[2] S. Sorrell, Reducing energy demand: a review of issues, challenges and approaches, Renew. Sust. Energ. Rev. 47 (1) (2015) 74–82.
[3] H.J. Akeiber, S.E. Hosseini, H.M. Hussen, M.A. Wahid, A.T. Mohammad, Thermal performance and economic evaluation of a newly developed phase change material for effective building encapsulation, Energy Convers. Manage. 150 (2017) 48–61.
[4] Y. Zhang, R. Wang, Sorption thermal energy storage: concept, process, applications and perspectives, Energy Stor. Mater. 27 (2020) 352–369.
[5] R. Wang, R. Oliveria, Adsorption refrigeration—an efficient way to make good use of waste heat and solar energy☆, Prog. Energy Combust. Sci. 32 (4) (2006) 424–458.
[6] Z. Ge, Y. Li, D. Li, Z. Sun, Y. Jin, C. Liu, C. Li, G. Leng, Y. Ding, Thermal energy storage: challenges and the role of particle technology, Particuology 15 (2014) 2–8.
[7] N. Yu, R.Z. Wang, L.W. Wang, Sorption thermal storage for solar energy, Prog. Energy Combust. Sci. 39 (5) (2013) 489–514.
[8] S. Song, L. Dong, Z. Qu, J. Ren, C. Xiong, Microencapsulated capric–stearic acid with silica shell as a novel phase change material for thermal energy storage, Appl. Therm. Eng. 70 (1) (2014) 546–551.
[9] L. Chen, J. Lv, L. Ding, G. Yang, Z. Mao, B. Wang, X. Feng, S. Zapotoczny, X. Sui, A shape-stable phase change composite prepared from cellulose nanofiber/polypyrrole/polyethylene glycol for electric-thermal energy conversion and storage, Chem. Eng. J. 400 (2020) 125950, https://doi.org/10.1016/j.cej.2020.125950.
[10] H. Zhang, J. Baeyens, G. Cáceres, J. Degrève, Y. Lv, Thermal energy storage: recent developments and practical aspects, Prog. Energy Combust. Sci. 53 (2016) 1–40.
[11] S. Becherini, M. Mitmoen, C.D. Tran, Biocompatible and smart composites from cellulose, wool, and phase-change materials encapsulated in natural sporopollenin microcapsules, ACS Sustain. Chem. Eng. 8 (27) (2020) 10089–10101.
[12] S. Kuravi, J. Trahan, D.Y. Goswami, M.M. Rahman, E.K. Stefanakos, Thermal energy storage technologies and systems for concentrating solar power plants, Prog. Energy Combust. Sci. 39 (4) (2013) 285–319.
[13] H. Zhang, F. Xing, H.-Z. Cui, D.-Z. Chen, X. Ouyang, S.-Z. Xu, J.-X. Wang, Y.-T. Huang, J.-D. Zuo, J.-N. Tang, A novel phase-change cement composite for thermal energy storage: Fabrication, thermal and mechanical properties, Appl. Energy 170 (2016) 130–139.
[14] L. Cao, D.i. Su, Y. Tang, G. Fang, F. Tang, Properties evaluation and applications of thermal energystorage materials in buildings, Renew. Sust. Energ. Rev. 48 (2015) 500–522.
[15] B. Pause, Phase change materials and their application in coatings and laminates for textiles, Smart Textile Coatings and Laminates (2019) 175–187.
[16] J. Giro-Paloma, M. Martínez, L.F. Cabeza, A.I. Fernández, Types, methods, techniques, and applications for microencapsulated phase change materials (MPCM): a review, Renew. Sust. Energ. Rev. 53 (2016) 1059–1075.
[17] Y. Li, S. Yu, P. Chen, R. Rojas, A. Hajian, L. Berglund, Cellulose nanofibers enable paraffin encapsulation and the formation of stable thermal regulation nanocomposites, Nano Energy 34 (2017) 541–548.
[18] X. Huang, X. Chen, A. Li, D. Atinafu, H. Gao, W. Dong, G.e. Wang, Shape-stabilized phase change materials based on porous supports for thermal energy storage applications, Chem. Eng. J. 356 (2019) 641–661.
[19] H. Peng, D. Zhang, X. Ling, Y. Li, Y. Wang, Q. Yu, X. She, Y. Li, Y. Ding, n-Alkanes phase change materials and their microencapsulation for thermal energy storage: a critical review, Energy Fuels 32 (7) (2018) 7262–7293.
[20] C. Liu, Z. Rao, J. Zhao, Y. Huo, Y. Li, Review on nanoencapsulated phase change materials: preparation, characterization and heat transfer enhancement, Nano Energy 13 (2015) 814–826.
[21] G. Fang, Z. Chen, H. Li, Synthesis and properties of microencapsulated paraffin composites with SiO2 shell as thermal energy storage materials, Chem. Eng. J. 163 (1-2) (2010) 154–159.
[22] S. Wu, T. Yan, Z. Kuai, W. Pan, Thermal conductivity enhancement on phase change materials for thermal energy storage: a review, Energy Stor. Mater. 25 (2020) 251–295.
[23] J.-F. Su, X.-Y. Wang, S. Han, X.-L. Zhang, Y.-D. Guo, Y.-Y. Wang, Y.-Q. Tan, N.-X. Han, W. Li, Preparation and physicochemical properties of microcapsules containing phase-change material with graphene/organic hybrid structure shells, J. Mater. Chem. A 5 (45) (2017) 23937–23951.
[24] B. Zhang, Z. Zhang, S. Kapar, P. Ataeian, J. da Silva Bernardes, R. Berry, W. Zhao, G. Zhou, K.C. Tam, Microencapsulation of phase change materials with polystyrene/cellulose nanocrystal hybrid shell via pickering emulsion polymerization, acs sustain, Chem. Eng. 7 (21) (2019) 17756–17767.
[25] J. Giro-Paloma, C. Barreneche, M. Martínez, B. Šumiga, A.I. Fernández, L. F. Cabeza, Mechanical response evaluation of microcapsules from different slurries, Renew. Energ. 85 (2016) 732–739.
[26] S. Puupponen, V. Mikkola, T. Ala-Nissila, A. Seppälä, Novel microstructured polyol–polystyrene composites for seasonal heat storage, Appl. Energy 172 (2016) 96–106.
[27] X. Du, Y. Fang, X.u. Cheng, Z. Du, M.i. Zhou, H. Wang, Fabrication and characterization of flame-retardant nanoencapsulated n-octadecane with melamine-formaldehyde shell for thermal energy storage, ACS Sustain. Chem. Eng. 6 (11) (2018) 15541–15549.
[28] Y. Yoo, C. Martinez, J.P. Youngblood, Synthesis and characterization of microencapsulated phase change materials with poly(urea-urethane) shells containing cellulose nanocrystals, ACS Appl. Mater. Interfaces 9 (37) (2017) 31763–31776.
[29] Y. Ahmadi, K.-H. Kim, S. Kim, M. Tabatabaei, Recent advances in polyurethanes as efficient media for thermal energy storage, Energy Stor. Mater. 30 (2020) 74–86.
[30] D.K. Döğüşcü, A. Altıntaş, A. Sarı, C. Alkan, Polystyrene microcapsules with palmitic-capric acid eutectic mixture as building thermal energy storage materials, Energy Build. 150 (2017) 376–382.
[31] R. Al-Shannaq, M. Farid, S. Al-Muhtaseb, J. Kurdi, Emulsion stability and cross-linking of PMMA microcapsules containing phase change materials, Sol. Energy Mater. Sol. Cells 132 (2015) 311–318.
[32] Y. Yang, Z. Fang, X. Chen, W. Zhang, Y. Xie, Y. Chen, Z. Liu, W. Yuan, An overview of pickering emulsions: Solid-particle materials classification, morphology, and applications, Front Pharmacol 8 (2017) 287.
[33] A. Chakrabarty, Y. Teramoto, Scalable pickering stabilization to design cellulose nanofiber-wrapped block copolymer microspheres for thermal energy storage, ACS Sustain. Chem. Eng. 8 (11) (2020) 4623–4632.
[34] Y. Chevalier, M.-A. Bolzinger, Emulsions stabilized with solid nanoparticles: pickering emulsions, Colloids Surf. A 439 (2013) 23–34.
[35] S.M. Andler, J.M. Goddard, Stabilization of lipase in polymerized high internal phase emulsions, J. Agric. Food. Chem. 66 (14) (2018) 3619–3623.
[36] X. Zhu, X. Li, J. Shen, B. Wang, Z. Mao, H. Xu, X. Feng, X. Sui, Stable microencapsulated phase change materials with ultrahigh payload for efficient cooling of mobile electronic devices, Energy Convers. Manage. 223 (2020) 113478.
[37] Z. Zhang, M. Cheng, M.S. Gabriel, Â.A. Teixeira Neto, J. da Silva Bernardes, R. Berry, K.C. Tam, Polymeric hollow microcapsules (phm) via cellulose nanocrystal stabilized pickering emulsion polymerization, J. Colloid Interface Sci. 555 (2019) 489–497.
[38] D. Gonzalez Ortiz, C. Pochat-Bohatier, J. Cambedouzou, M. Bechelany, P. Miele, Current trends in pickering emulsions: particle morphology and applications, Engineering 6 (4) (2020) 468–482.
[39] T.D. Dao, H.M. Jeong, A pickering emulsion route to a stearic acid/graphene core–shell composite phase change material, Carbon 99 (2016) 49–57.
[40] D. Yin, L. Ma, J. Liu, Q. Zhang, Pickering emulsion: a novel template for microencapsulated phase change materials with polymer–silica hybrid shell, Energy 64 (2014) 575–581.
[41] H. Wang, L. Zhao, G. Song, G. Tang, X. Shi, Organic-inorganic hybrid shell microencapsulated phase change materials prepared from SiO2/TiC-stabilized pickering emulsion polymerization, Sol. Energy Mater. Sol. Cells 175 (2018) 102–110.
[42] Y. He, F. Wu, X. Sun, R. Li, Y. Guo, C. Li, L.u. Zhang, F. Xing, W. Wang, J. Gao, Factors that affect pickering emulsions stabilized by graphene oxide, ACS Appl. Mater. Interfaces 5 (11) (2013) 4843–4855.
[43] Q. Zhao, W. Yang, H. Zhang, F. He, H. Yan, R. He, K. Zhang, J. Fan, Graphene oxide pickering phase change material emulsions with high thermal conductivity and photo-thermal performance for thermal energy management, Colloids Surf. A 575 (2019) 42–49.
[44] I. Capron, B. Cathala, Surfactant-free high internal phase emulsions stabilized by cellulose nanocrystals, Biomacromolecules 14 (2) (2013) 291–296.
[45] X. Li, J. Li, J. Gong, Y. Kuang, L. Mo, T. Song, Cellulose nanocrystals (CNCs) with different crystalline allomorph for oil in water pickering emulsions, Carbohydr. Polym. 183 (2018) 303–310.

[46] H. Dupont, C. Fouche, M.A. Dourges, V. Schmitt, V. Heroguez, Polymerization of cellulose nanocrystals-based Pickering HIPE towards green porous materials, Carbohydr. Polym. 243 (2020), 116411.
[47] H. Dai, J. Wu, H. Zhang, Y. Chen, L. Ma, H. Huang, Y. Huang, Y. Zhang, Recent advances on cellulose nanocrystals for Pickering emulsions: development and challenge, Trends Food Sci. Technol. 102 (2020) 16–29.
[48] Z. Zhang, K.C. Tam, X. Wang, G. Sèbe, Inverse pickering emulsions stabilized by cinnamate modified cellulose nanocrystals as templates to prepare silica colloidosomes, ACS Sustain. Chem. Eng. 6 (2) (2018) 2583–2590.
[49] C. Salas, T. Nypelö, C. Rodriguez-Abreu, C. Carrillo, O.J. Rojas, Nanocellulose properties and applications in colloids and interfaces, Curr. Opin. Colloid Interface Sci. 19 (5) (2014) 383–396.
[50] I. Kalashnikova, H. Bizot, B. Cathala, I. Capron, Modulation of cellulose nanocrystals amphiphilic properties to stabilize oil/water interface, Biomacromolecules 13 (1) (2012) 267–275.
[51] F. Wang, Y. Zhang, X. Li, B. Wang, X. Feng, H. Xu, Z. Mao, X. Sui, Cellulose nanocrystals-composited poly (methyl methacrylate) encapsulated n-eicosane via a Pickering emulsion-templating approach for energy storage, Carbohydr. Polym. 234 (2020), 115934.
[52] H. Cui, H. Chen, Z. Guo, J. Xu, J. Shen, Preparation of high surface area mesoporous melamine formaldehyde resins, Microporous Mesoporous Mater. 309 (2020) 110591, https://doi.org/10.1016/j.micromeso.2020.110591.
[53] J. Li, Q. Li, L.-S. Li, L.i. Xu, Removal of perfluorooctanoic acid from water with economical mesoporous melamine-formaldehyde resin microsphere, Chem. Eng. J. 320 (2017) 501–509.
[54] F. Luo, K. Wu, S. Wang, M. Lu, Melamine resin/graphite nanoflakes hybrids and its vacuum-assisted prepared epoxy composites with anisotropic thermal conductivity and improved flame retardancy, Compos. Sci. Technol. 144 (2017) 100–106.
[55] G. Ming, H. Duan, X. Meng, G. Sun, W. Sun, Y.u. Liu, L. Lucia, A novel fabrication of monodisperse melamine–formaldehyde resin microspheres to adsorb lead (II), Chem. Eng. J. 288 (2016) 745–757.
[56] Y. Wu, Y. Li, L. Qin, F. Yang, D. Wu, Monodispersed or narrow-dispersed melamine-formaldehyde resin polymer colloidal spheres: preparation, size-control, modification, bioconjugation and particle formation mechanism, J. Mater. Chem. B 1 (2) (2013) 204–212.
[57] D.J. Merline, S. Vukusic, A.A. Abdala, Melamine formaldehyde: curing studies and reaction mechanism, Polym. J. 45 (4) (2012) 413–419.
[58] Q. Zhang, Y. Zhao, J. Feng, Systematic investigation on shape stability of high-efficiency SEBS/paraffin form-stable phase change materials, Sol. Energy Mater. Sol. Cells 118 (2013) 54–60.
[59] H.-Y. Wu, S.-T. Li, Y.-W. Shao, X.-Z. Jin, X.-D. Qi, J.-H. Yang, Z.-W. Zhou, Y. Wang, Melamine foam/reduced graphene oxide supported form-stable phase change materials with simultaneous shape memory property and light-to-thermal energy storage capability, Chem. Eng. J. 379 (2020) 122373, https://doi.org/10.1016/j.cej.2019.122373.
[60] M.H. Zahir, S.A. Mohamed, R. Saidur, F.A. Al-Sulaiman, Supercooling of phase-change materials and the techniques used to mitigate the phenomenon, Appl. Energy 240 (2019) 793–817.
[61] X.-X. Zhang, X.-M. Tao, K.-L. Yick, X.-C. Wang, Structure and thermal stability of microencapsulated phase-change materials, Colloid. Polym. Sci. 282 (4) (2004) 330–336.
[62] C. Devallencourt, J.M. Saiter, A. Fafet, E. Ubrich, Thermogravimetry/Fourier transform infrared coupling investigations to study the thermal stability of melamine formaldehyde resin, Thermochim. Acta 259 (1) (1995) 143–151.